ACS MATERIALS LETTERS

www.acsmaterialsletters.org

Nanophase-Separated Block-co-Polymers Based on Phosphonated Pentafluorostyrene and Octylstyrene for Proton-Exchange Membranes

Sebastian Auffarth,* Maximilian Wagner, Anja Krieger, Birk Fritsch, Linus Hager, Andreas Hutzler, Thomas Böhm, Simon Thiele, and Jochen Kerres*

Cite This: *ACS Materials Lett.* 2023, 5, 2039–2046

Read Online

ACCESS | Metrics & More | Article Recommendations | Supporting Information

ABSTRACT: Nanophase separation into hydrophobic and hydrophilic domains in commercial perfluorosulfonic acid polymers promotes high conductivity by forming proton-conductive channels within a matrix. To transfer this beneficial phase separation to phosphonic acid functionalized ionomers, we combine phosphonated polypentafluorostyrene and flexible polyoctylstyrene in a di-block-co-polymer. We introduce a stepwise approach, including mesophase simulations, synthesis, and spectroscopic imaging. After the required block lengths were calculated, controlled radical polymerization led to a narrowly distributed block-co-polymer. The respective block-co-polymer membrane outperforms a phosphonated pentafluorostyrene blend concerning conductivity and water uptake. Stained membrane cross-sections revealed bicontinuous nanophase separation in the 13 to 25 nm range in transmission electron microscopy. The ion-conducting phosphonated polymer block assembled into an isotropic, three-dimensional gyroidal network across the membrane. Our stepwise approach is transferable toward other block-co-polymer systems featuring different monomers or functional groups. Applying the proposed principles allows for the prediction of structure-related phase separation while reducing the amount of synthesis work.

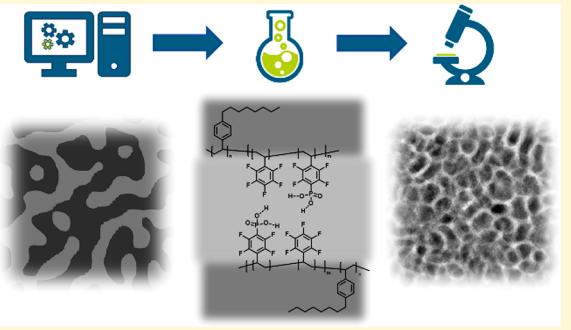

Ion-conducting polymers (ionomers) are part of a wide range of electrolyzers, batteries, and fuel cells, facilitating ion transport between anode and cathode reactions.[1−3] In those applications, their high ion conductivity can be utilized in membranes and electrodes.[4,5] Application-relevant ionomer properties include

- high conductivity at application temperature
- high chemical stability against the reactants/products, radicals, humidity and temperature(-changes)
- high durability against dimensional changes related to swelling, start/shut-down cycles, and pressure deviations in reactant/product feeds

If an ionomer is used as a membrane material, the electric insulation of the anode and cathode, the separation of the reactants and the selective transport of different ionic species are essential.[6−8] Ionomer membranes can be specifically tailored for their respective applications, because of the broad range of possible material modifications.

Nafion and its derivates have emerged as standard materials for hydrogen fuel cells and electrolyzers featuring a fluorinated, aliphatic polymer backbone and sulfonic acid group side chains.[9−11] In particular, Nafion excels in achieving high proton conductivities despite a comparably low ion-exchange capacity (IEC) of under one mmol H^+ per gram of polymer. This characteristic relates to a pronounced phase separation in the nanometer range, promoting channels with high local concentrations of water and sulfonic acid.[12,13] Compared to randomly sulfonated copolymers, phase separation of block-co-polymers enhances the conductivity, water uptake, and cell performance.[14,15] Recently, the thiolation of block-co-polymers

Received: May 30, 2023
Accepted: June 20, 2023

https://doi.org/10.1021/acsmaterialslett.3c00569
ACS Materials Lett. 2023, 5, 2039−2046

from polypentafluorostyrene (PPFS) and butylacrylate enabled the preparation of thin films and membranes with distinct nanophase separation between 30 and 96 nm.[16,17] Extensive swelling of the mercaptopropane sulfonate functionalized ionomer was observed in water, but ionic and covalent cross-linking stabilized the membranes.[17]

In general, the presence of water around acidic groups enables high proton conductivity due to distinct hopping and vehicular transport mechanisms.[18] Above 100 °C at ambient pressure, the evaporation of water limits the sufficient humidification of sulfonated polymers required for high conductivities.

Consequently, high-temperature applications above 100 °C often rely on phosphoric acid-doped membranes.[19] The respective ionomers contain a positive or protonated group, which coordinates phosphoric acid and phosphonates.[20,21] General obstacles of phosphonic acid-doped materials include catalyst poisoning by phosphonate anions and acid loss over time.[22,23] The loss of the ion-conducting acid can occur during operation by evaporation above 160 °C or via an exponential water replacement mechanism.[24] Phosphonic acid groups can also be directly attached to a polymer to avoid acid loss over time. In phosphonated polypentafluorostyrene (PWN), the electron-deficient aromatic ring enhances the acidity of the ion-conducting group by stabilizing the corresponding negative charge.[25] Applying atom-transfer radical polymerization, first graft and block-co-polymers of PWN have been reported based on polymer backbones with high molecular weight dispersity and glass transition temperature.[26−28] Unfortunately, PWN, in its dry state, is also very brittle due to its high glass-transition temperature.[29] The mechanical properties can be enhanced by blending them with polybenzimidazole. While the additional acid−base cross-links further stabilize the membrane, the basic benzimidazole groups reduce the number of accessible acid groups for proton transport.

In this publication, we present the mesophase structure simulation-supported, controlled synthesis of a block-co-polymer based on brittle PWN and viscous polyoctylstyrene (POS). After preparation of a diblock-polymer membrane, the conductivity and water uptake were determined. The nanostructure of the membrane was analyzed by scanning transmission electron microscopy (STEM) and energy-dispersive X-ray spectroscopy (EDXS).

Various solubility parameters can describe the interactions between two blocks within a di-block-co-polymer. In this publication, solubility parameters and molar densities were calculated by forcite calculations (see SI-1). Table 1 shows the respective densities and solubility parameters of different repeating units calculated from an energy minimization of 100 monomers each. We decided to reduce the phosphonation degree to two-thirds in the simulation since fully phosphonated PWN-100 is water-soluble.[25] Figure 1 depicts the nanophase separation from mesostructured simulations of di-block-co-polymers with various lengths based on partly phosphonated PWN and POS in 64·64·64 nm^3 cubes. The number of simulated polymer chains is related to the block lengths and their molar volume (see SI-1). Typical for di-block-co-polymers, the ratio between the block lengths of partly phosphonated PWN and POS plays a significant role in the nanostructure. A continuous nanophase of functional groups is required to ensure sufficient conductivity of charges within ion exchange membranes.

Table 1. Calculated Parameters for Mesostructure Simulations by Forcite Energy Minimization

polymer	solubility parameter [(J cm^{-3})$^{0.5}$]	density [g cm^{-3}]	molar mass [g mol^{-1}]	molar volume [cm^3 mol^{-1}]
phosphonated PFS	24.0	1.6	256	160
pentafluorostyrene	18.6	1.42	194	137
octylstyrene	17.2	0.85	216	254
PWN-66	22.2	1.54	235	152
PWN-66-POS	5.0			203

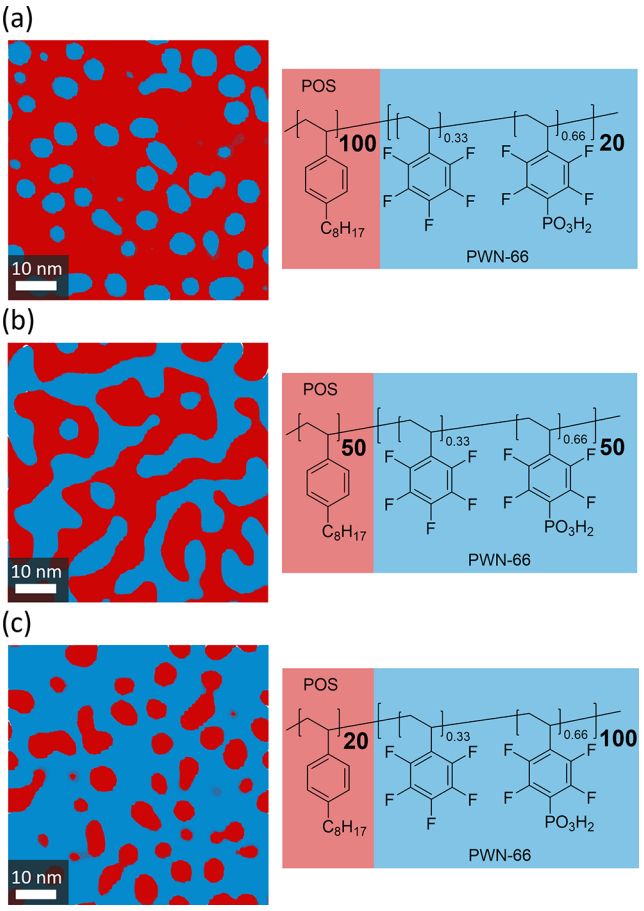

Figure 1. Mesostructure simulations of nanophase separation of POS-b-PWN-66 with block lengths of 100:20 (a), 50:50 (b), and 20:100 (c). The simulated cubes consist of 5543 (a), 7763 (b), 7769 (c) distinct POS-b-PWN-66 chains.

For proton-exchange membranes, a continuous domain of phosphonic acid groups presents a direct pathway for protons to move through the membrane. Therefore, materials with nanophase separations, as depicted in Figure 1b and c, promise sufficient conductivity. A bicontinuous system, like in Figure 1b, offers adequate conductivity while reducing the amount of brittle PWN. The length adjustment of the polymer blocks allows fine-tuning of the nanophase. Thus, the simulations of this relationship are utilized in the following polymer synthesis.

The mesostructure simulations of the POS-b-PWN-66 derivatives rely on distinct block lengths with a unique molecular weight. Therefore, we aimed to synthesize polymers with a narrow polymer weight distribution to minimize a potential impact on the nanophase separation. The stepwise polymerization of the di-block-co-polymer was realized by a controlled radical polymerization utilizing a reversible addition-fragmentation chain-transfer (RAFT) reagent. Figure 2 shows the synthesis of the block-co-polymer POS-PPFS and the

https://doi.org/10.1021/acsmaterialslett.3c00569
ACS Materials Lett. 2023, 5, 2039−2046

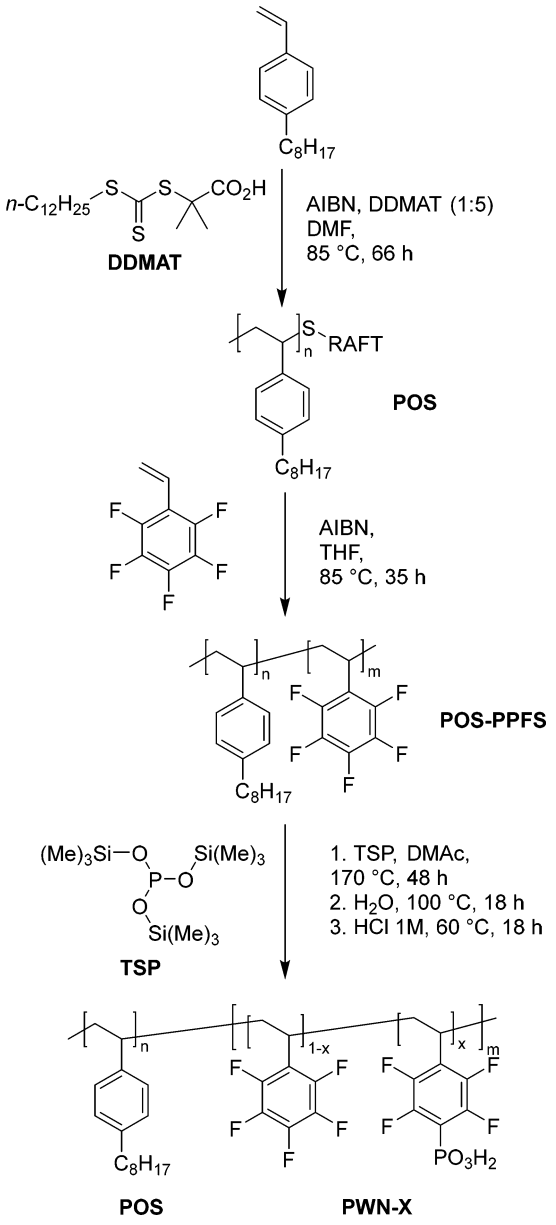

Figure 2. Stepwise synthesis of POS-PPFS by RAFT-polymerization and partial phosphonation.

subsequent phosphonation of X% pentafluorostyrene units to POS-PWN-X. End-group and backbone analyses by nuclear magnetic resonance (NMR) spectroscopy (see SI-2) and size-exclusion chromatography (GPC) were used to calculate the block lengths within the di-block-co-polymer POS-PPFS (Table 2).

While only the synthesis of the first block POS required an additional RAFT reagent, azobis(isobutyronitrile) (AIBN) initiated the polymerizations of both polymer blocks. The RAFT-terminated POS was isolated as a yellow, sticky oil since the alkyl chains in the para-position disturb POS's crystallization, lowering the glass transition temperature.[30] For calculation of the block lengths, the degree of polymerization (DP, average number of monomer units per polymer) was determined. The terminal CH_3-group of the RAFT reagent was used as a reference for calculating the block length by ^{1}H-NMR analysis (see SI-2). Compared to the block length by end-group analysis, GPC's mass average corresponds to a slightly higher number of octylstyrene units. Next to minor chain termination by recombination, this finding relates to GPC's polystyrene standard calibration and the increased hydrodynamic diameter of POS.

Nevertheless, the low dispersity of under 1.04 underlines the narrow weight distribution of the controlled radical polymerization. For the second block of PPFS, the POS block was utilized as a macro-RAFT-reagent. By comparing backbone integrals, NMR analysis proves the successful synthesis of the di-block-co-polymer POS-b-PPFS with equal block sizes (see SI-2). Deriving the difference in mass average from GPC, the block lengths for the PPFS block are similar regardless of the analysis technique. While the dispersity of POS-b-PPFS increased slightly, the diblock exhibits the expected glass transition temperatures of around −20 and 100 °C (see SI-4).[31,32]

The PPFS part of the diblock-polymer was phosphonated by para-fluor substitution with tris(trimethylsilyl)-phosphite (TSP). The stoichiometric equivalents of the TSP influence the phosphonation degree X, as described in the literature for the phosphonation of pure PPFS.[33] Additional factors that impact the phosphonation degree include influences of additional solvent and water/oxygen impurities, which quench the TSP during or before the reaction. To monitor the phosphonation degree X against time, we traced the reaction by ^{19}F-NMR (see SI-3). Since TSP substitutes the para-fluorine atom, the degree of phosphonation can be calculated from the integrals of the respective peaks. The solvent DMAc seemed to limit the phosphonation degrees to around 60% despite 1.2 equiv of TSP. During the subsequent workup, the protecting groups were hydrolyzed. For higher phosphonation degrees, pure TSP was used both as a reactant and as a solvent for POS-b-PPFS. The excess of TSP leads to shorter reaction times of a few hours (see SI-3). However, (nearly) complete phosphonation of PWN-homopolymers causes water solubility, preventing their application in aqueous conditions. A fully phosphonated POS-b-PWN-100 derivate showed good film-forming properties but disintegrated into a turbid dispersion due to the excessive water uptake of the PWN-100 block.

The block-co-polymer POS-b-PWN-60 forms a clear, viscous gel in dimethylsulfoxide (DMSO). By the addition of tetrahydrofuran (THF), the viscosity of the polymer solution decreases drastically to allow membrane manufacturing by solution casting. This observation relates to the different solubilities of the hydrophobic and hydrophilic blocks. Unlike pristine PWN, the POS-b-PWN-60 membrane features two glass transition temperatures at −20 and 265 °C (see SI-4). The membrane POS_{50}-b-$PWN\text{-}60_{54}$ is relatively sticky to various

Table 2. Block Lengths from GPC/NMR Analysis and Glass Transition Temperatures of Block-co-polymer POS-b-PPFS

polymer-block	M_n/M_w [kg mol^{-1}]	dispersity Đ	block length GPC-M_w	block length ^{1}H-NMR	T_g [°C]
polyoctylstyrene (POS)	12.8/13.3	1.037	62	50	
polypentafluorostyrene (PPFS)			55	54	
POS-b-PPFS	21.1/24.0	1.137			−19/101

https://doi.org/10.1021/acsmaterialslett.3c00569
ACS Materials Lett. 2023, 5, 2039−2046

surfaces, such as a polyethylene storage bag. When the POS ratio in the presented block-co-polymer is increased, the stickiness is expected to increase until the membrane becomes a viscous oil. When the PPFS block is enlarged to around 185 units, the water uptake of the PWN part, which is responsible for membrane disintegration, needs to be contradicted. The phosphonation degree was reduced to 42%. While the decreased proportion of POS reduced the stickiness of POS_{50}-b-$PWN\text{-}42_{185}$, the general mechanical handling of the membrane was similar to POS_{50}-b-$PWN\text{-}60_{54}$. The material's brittleness corresponds to Young's modulus, which was analyzed by dynamic mechanical analysis (see SI-5). As expected, pure PWN-75 has a higher Young's modulus of 275 ± 42 MPa than the POS-b-PWN-60 with 70 ± 7 MPa at 0% relative humidity. With its −20 °C glass transition temperature, the POS block softens the respective membrane, resulting in a lower overall brittleness/Young's modulus. At high relative humidities of around 90% (maximum of our testing device), the Young's moduli of PWN-75 and POS-b-PWN-60 are very close within the same order of magnitude and decrease by 98.6% and 89.3%, respectively. Since their high phosphonation degree, PWN-75 and POS-b-PWN-60 absorb water, significantly lowering the brittleness. However, the absolute change is lower for POS-b-PWN-60 because the POS block causes a general softening regardless of the precise relative humidity. While these results prove the softening effect of the flexible POS on the brittle PWN, additional cross-linking of the polymer chains may be incorporated in the future to achieve elastomeric properties of the block-co-polymer.

Table 3 compares the POS-b-PWN-60 membrane's properties (see experimental details in SI-6) to Nafion and a blend of PWN-75 and polyvinylidene fluoride (PVDF). The through-plane membrane conductivities at room temperature of POS-b-PWN-60 and the PVDF-PWN-75-blend are lower than for the commercial Nafion 211 reference. This finding is expected and relates to the lower acidity of phosphonic acid groups compared with the sulfonic acids found in Nafion. Like phosphoric acid, phosphonated ionomers can simultaneously act as a proton acceptor and donor, reducing reliance on water to ensure proton conductivity.[34,35] The phosphonated PWN also features higher thermal stability than the sulfonated equivalent ($T_{degradation}$: 391 °C for PWN/351 °C for sulfonated PPFS).[36] Phosphonated ionomers are therefore used in low humidity applications, especially.[37] A higher number of acidic groups generally increase the number of charge carriers in proton-exchange membranes, thereby enhancing conductivity. The ratio of the PVDF and PWN-75 was set to mimic the number of charge carriers (IEC_{direct}) of POS-PWN-60 to allow a direct comparison of conductivity and swelling. Despite their same IEC_{direct} (see experimental details in SI-6), POS-b-PWN-60 has a 50% higher conductivity than the PVDF-PWN-75. As for Nafion, distinct nanophase separation produces pathways for proton transport by locally increasing the concentration of acidic groups. The PVDF-PWN-75-membrane has a far higher water uptake of 123 wt % at 85 °C, whereas the uptake of Nafion and POS-b-PWN-60 is around 40 wt % and 70 wt % (see Table 3). While the water uptake is higher than for commercial Nafion membranes, the nonpolar POS block reduces the water uptake of POS-b-PWN-60 significantly compared to PVDF-PWN-75.

Table 3. Membrane Properties of POS-b-PWN-60, PVDF-PWN-75, and Nafion 211

membrane	conductivity [mS cm^{-1}]	water uptake (wt %) at 25/60/85 °C	IEC_{direct} [mmol g^{-1}]
POS-b-PWN-60	33 ± 2	27/44/71	1.22
PVDF-PWN-75	21 ± 1	44/69/123	1.25
N211	55 ± 4	15/36/41	0.91*

*Calculated from the equivalent weight.

In general, high water absorption directly correlates with dimensional swelling and wider proton conductive channels. Despite the lower water uptake of POS-b-PWN-60, the additional nanostructure increases the local density of the proton conducting groups. This effect seems to overcompensate for the influence of the reduced water absorption on the conductivity. In literature, the impact of the copolymer architecture on the conductivity in regard to hydration has been demonstrated for different sulfonated membranes before.[38,39] A sulfonated block copolymer from styrene and isobutylene polymer (48% sulfonation degree, IEC_{direct} 1.28 mmol g^{-1}) featured a conductivity at room temperature of around 25 mS cm^{-1} and a water uptake of 75 wt % (Nafion 117: 27 mS cm^{-1}, 25 wt %).[14] Utilizing an in-plane conductivity procedure, a copolymer consisting of PVDF/hexafluoropropylene and partially sulfonated styrene blocks with an IEC_{direct} of 1.18 mmol g^{-1} had a conductivity of 80 mS cm^{-1} and a water-uptake of around 90 wt % (Nafion 117: 72 mS cm^{-1}, 29 wt %).[40] While the conductivities of sulfonated, phase-separated membranes equal that of their respective Nafion references, the water uptake at room temperature was significantly higher than that for POS-b-PWN-60. Compared to the phosphonated PVDF-PWN-75 blend, the block-co-polymer membrane features a conductivity increase of 50% despite a 40% decrease in swelling. These results clearly show the potential of our block-co-polymer approach toward high-performance membrane alternatives. The sulfonation of the block-co-polymer is currently being investigated in our laboratories to provide nanostructure-enhanced membranes for low-temperature applications.

To prove the formation of distinct nanophases, the POS-b-PWN-60 membrane was stained with Pb^{2+}-ions and an ultramicrotomy cross-section was analyzed by high-angle annular dark field (HAADF) STEM imaging. Pb^{2+}-staining increases the Z-contrast in HAADF-STEM due to the Rutherford-like scattering. The HAADF-STEM micrographs in Figure 3 depict a clear nanophase separation of a bright, continuous, honeycomb-like structure within a darker phase. Nanophases with highly polar constituents, like the polar PWN-60 block, accumulate the charged Pb^{2+}-ions while they are excluded from the nonpolar POS block. As the scattering at the Pb^{2+}-ions creates a bright image contrast, the darker domains correspond to the POS block.

As mentioned, the dark and bright domains consist of nonpolar and polar blocks, respectively. The different shades within the TEM images (e.g., visible in Figure 3a) can be explained by the section thickness of the sample, with a nominal thickness of 75 nm. Consequently, the transmission images contain overlaps between polar and nonpolar domains. The interconnection of bright domains between dark, nonpolar domains forms a gyroidal, three-dimensional network. Since this network consists of the polar PWN-60 block, isotropic proton transport occurs through the phosphonic groups. In contrast, lamellar or similar nanophases often align parallel to the fabrication direction (here, membrane casting), negatively affecting the perpendicular through-plane conductivity.[41]

https://doi.org/10.1021/acsmaterialslett.3c00569
ACS Materials Lett. 2023, 5, 2039−2046

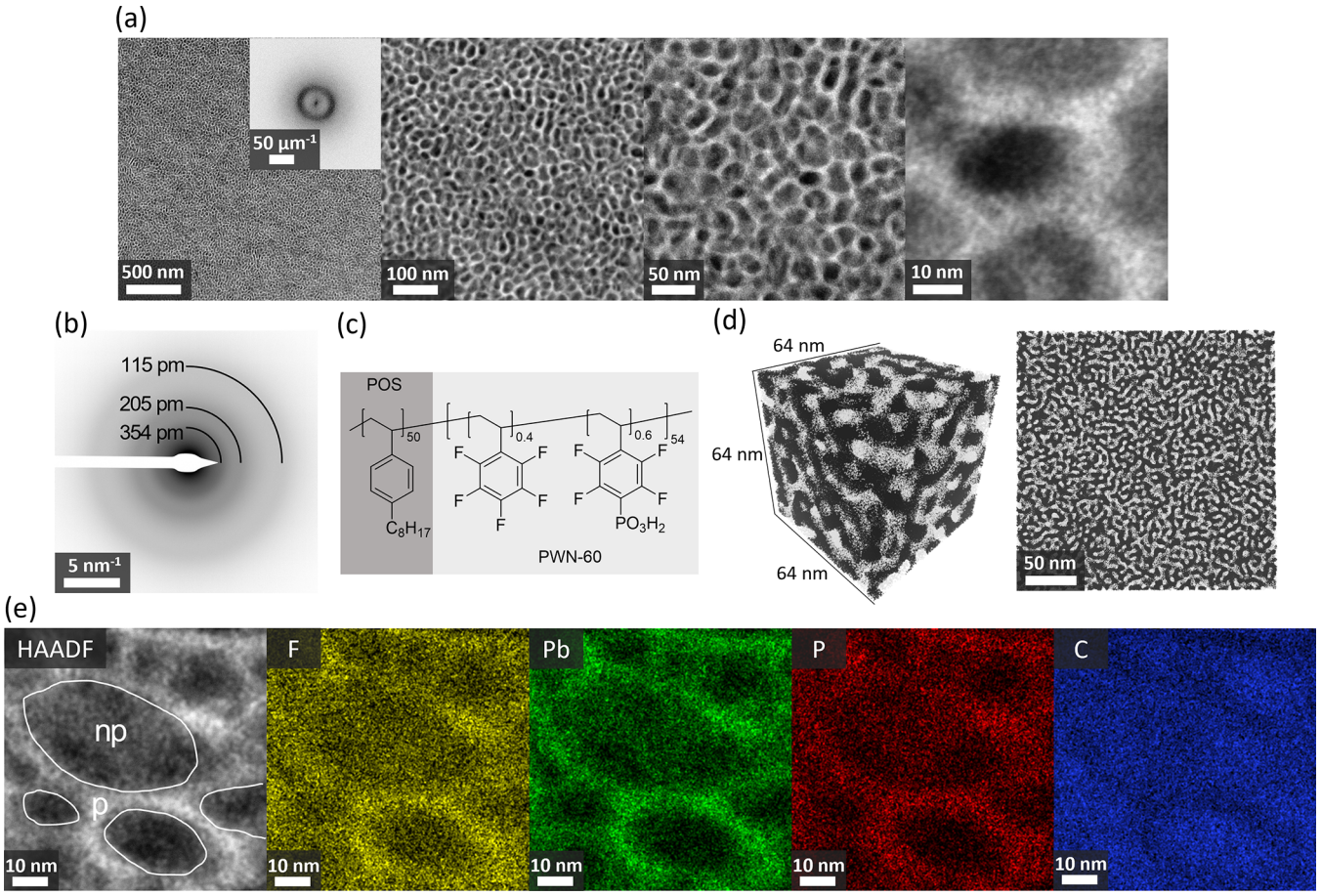

Figure 3. Nanophase separation in POS-b-PWN-60. (a) HAADF-STEM images of the Pb^{2+} stained membrane cross-section and diffractogram for nanostructure size determination. (b) Mean atomic-bond lengths from SAED. (c) Chemical structure of the polymer from synthesis. (d) Nanophase simulation of POS_{50}-b-$PWN\text{-}66_{50}$ with the same parameters as those in Figure 1. Similar to (a), the dark parts correspond to the nonpolar POS-rich phase. (e) Structure domains highlighted in HAADF image and corresponding EDXS images for fluorine, lead, phosphorus, and carbon.

At high magnification, the bright intensity at the interphase between the nonpolar and polar domains only decays gradually. This observation may be explained by staining artifacts and ultimately hinders the direct measurement of domain sizes from STEM images. Therefore, the average sizes of the domains were extracted from the diffractograms (see inset in Figure 3a) of the HAADF-STEM images. The nonpolar regions have an average size of 24.7 ± 9.5 nm, whereas polar domains are slightly smaller with an average size of 12.7 ± 2.5 nm (marked as np/p in Figure 3e, respectively). In addition, a nanostructure size of 2.3 ± 1.3 nm (visible in Figure 3a at higher magnification) was extracted, which might relate to agglomerations of octylstyrene repeating units or the congregation of multiple phosphonic acid groups within the polar region. Additional selected area electron diffraction (SAED) was performed to obtain information about potential smaller structure sizes. The corresponding selected area bright field TEM micrograph is depicted in SI-7. By least-squares fitting of background-corrected, polar-integrated radial intensity profiles,[42] structure sizes in the range of various inter-/intramolecular bond lengths were identified (see Figure 3b).

Compared to the simulation of an ideal 50−50 co-block-polymer (Figure 3d), the cross-section of the actual polymer POS-b-PWN-60 (chemical structure depicted in Figure 3c) appears to have slightly larger domain sizes. Although still on the same order of magnitude, the deviation in the transmission images also relates to the domain's random orientation within the sample section and blurred domain edges (see SI-8). Slight deviations from a broader polymer weight distribution and lower phosphonation might also influence the precise form of the nanophases in the STEM micrographs. The observed honeycomb structure of the polar domains could relate to other interactions within the distinct nanophases, which were not considered in the simulation. Nevertheless, our mesophase simulations of diblock polymers accurately predicted the bicontinuous, phase-separated structure and successfully guided our polymer synthesis.

Additional EDXS imaging in Figure 3e confirms the assignment of POS and PWN-60 domains. The intensities of fluorine and phosphorus, only present in the PWN-60 block, correlate with the bright regions of the micrographs. As expected, the intensity of the lead emerges in the same regions, highlighting the polarity of the phases. In contrast, differences in carbon intensity, present in both parts of the block-co-polymer, are minor. The higher fraction of carbon in the POS block (89 wt % C) compared to the PWN-60 block (42 wt % C without lead staining) results in slightly higher intensity in the nonpolar domains.

To conclude, we present the combination of simulation, synthesis, and (spectroscopic) imaging of a block-co-polymer for application as a proton-exchange membrane. After

https://doi.org/10.1021/acsmaterialslett.3c00569
ACS Materials Lett. 2023, 5, 2039−2046

calculating the solubility parameters for mesostructure analysis, we estimated the required block sizes for a bicontinuous polymer nanophase. Controlled RAFT-polymerization allowed us to realize the proposed diblock backbone structure with two distinct glass transition temperatures. After partial phosphonation, membranes were manufactured by solution casting. Compared with a PWN75-PVDF blend, the diblock-polymer exhibited improved conductivity and water uptake. The proposed nanostructure of a cross-section was verified by HAADF-STEM imaging and EDXS, where a gyroidal network of ion-conducting domains was found. The isotropic distribution of these domains enables a high ion conductivity. In the future, our simulation-guided synthesis approach may help in the manufacture of membranes from ionomers suffering from high brittleness. We look forward to expanding our block-co-polymer systems to other nonpolar polymer blocks and further ion-conducting functional groups.

EXPERIMENTAL METHODS

Octylstyrene was destabilized by an alumina oxide column. All of the other chemicals were used without further purification.

Synthesis of the Block-co-polymer POS-PPFS. DDMAT (97.0 mg, 0.26 mmol, 1 equiv) and AIBN (8.7 mg, 0.05 mmol, 0.2 equiv) were dissolved in a mixture of DMF (3 mL) and 4-*n*-octylstyrene (4.5 g, 5.4 mL, 0.02 mol, 80 equiv), and the reaction mixture was degassed by three freeze−pump−thaw cycles to remove oxygen residuals. The reaction mixture was stirred at 85 °C for three days. The viscous yellow raw product was dissolved in ethyl acetate (10 mL) and precipitated in methanol twice. The viscous oil was separated, and volatile residual solvents/monomer were removed at 80 °C under high vacuum. The poly(4-octylstyrene) (POS, macro-chain-transfer-reagent, 2.2 g, 0.18 mmol, 1 equiv) was dissolved in destabilized THF and was added to 1,2,3,4,5-pentafluorostyrene (2.1 g, 1.5 mL, 0.01 mol, 60 equiv) and AIBN (6.0 mg, 0.04 mmol, 0.2 eq). The reaction mixture was stirred at 85 °C for 35 h. The viscous solution was diluted in THF (5 mL) and precipitated in isopropanol twice. The yellowish powder POS-PPFS (2.1 g) was filtered off and dried overnight at 60 °C in a vacuum oven.

Phosphonation of the Block-co-polymer POS-PPFS. For partial phosphonation, POS-PPFS (2.0 g, 5.19 mmol PFS-units, 1 equiv) was dissolved in DMAc, and the phosphonation reagent TSP (2.0 g, 2.3 mL, 0.07 mmol, 1.26 equiv) was added portion-wise. Under an argon atmosphere, the reaction mixture was heated to 170 °C for 48 h. For full phosphonation, POS-PPFS (1 equiv) can be dissolved in the phosphonation reagent TSP (6 eq). Under an argon atmosphere, the reaction mixture was heated up to 170 °C for 20 h. In both cases, the crude product was cooled to room temperature and precipitated in acetonitrile. The polymer was filtered off and consecutively hydrolyzed in water (100 °C) and aqueous HCl (1 M, 60 °C) for one day each. The polymer suspension was precipitated once in acetonitrile and washed with water until a neutral pH. The phosphonated polymer POS-PWN-60 was dried at 95 °C for 18 h and at 60 °C for 2 h in a vacuum oven to yield a yellow solid (1.3 g).

Membrane Casting. After dissolving the di-block-co-polymer in DMSO (5 wt % solution), THF (20 wt %) was added to the solution to decrease the viscosity for doctor blade casting. After adding THF to the viscous polymer solution in DMSO (5 wt %), the final polymer concentration is around 4.2 wt %. The casted thin film was predried sequentially at 45 and 65 °C for 45 min each to evaporate the THF slowly. After, the thin film was dried at 85 °C for 2 h. To ensure complete evaporation of the solvent, the membrane was further dried at 110 °C overnight. A gap height of 900 μm resulted in a 32 μm thick membrane after detachment in water. The PVDF-PWN-75 blend membranes were prepared by mixing PVDF (10 wt %) and PWN-75 (5 wt %) solutions in DMAc. The PWN-75 was synthesized according to the literature.[25] The ratio of PVDF and PWN-75 was calculated according to the measured IEC_{direct} of the membrane POS-PWN-60.

ASSOCIATED CONTENT

Supporting Information

The Supporting Information is available free of charge at https://pubs.acs.org/doi/10.1021/acsmaterialslett.3c00569.

Simulation of POS-PWN-66 nanophase; NMRs of the block-co-polymers; DSC curves of POS-PPFS and POS-PWN60; DMA measurements of POS-b-PWN-60 and PWN-75; experimental details of membrane characterization; experimental details of nanophase imaging; analysis of STEM and simulation images of POS-PWN; NMR and GPC methods (PDF)

AUTHOR INFORMATION

Corresponding Authors

Sebastian Auffarth − *Forschungszentrum Jülich GmbH, Helmholtz Institute Erlangen-Nürnberg for Renewable Energy (IEK 11), 91058 Erlangen, Germany; Department of Chemical and Biological Engineering, Friedrich-Alexander-Universität Erlangen-Nürnberg, 91058 Erlangen, Germany;* orcid.org/0000-0002-6784-9135; Email: s.auffarth@fz-juelich.de

Jochen Kerres − *Forschungszentrum Jülich GmbH, Helmholtz Institute Erlangen-Nürnberg for Renewable Energy (IEK 11), 91058 Erlangen, Germany; Chemical Resource Beneficiation Faculty of Natural Sciences, North-West University, Potchefstroom 2520, South Africa*; Email: j.kerres@fz-juelich.de

Authors

Maximilian Wagner − *Forschungszentrum Jülich GmbH, Helmholtz Institute Erlangen-Nürnberg for Renewable Energy (IEK 11), 91058 Erlangen, Germany*

Anja Krieger − *Forschungszentrum Jülich GmbH, Helmholtz Institute Erlangen-Nürnberg for Renewable Energy (IEK 11), 91058 Erlangen, Germany*

Birk Fritsch − *Forschungszentrum Jülich GmbH, Helmholtz Institute Erlangen-Nürnberg for Renewable Energy (IEK 11), 91058 Erlangen, Germany;* orcid.org/0000-0001-7935-2188

Linus Hager − *Forschungszentrum Jülich GmbH, Helmholtz Institute Erlangen-Nürnberg for Renewable Energy (IEK 11), 91058 Erlangen, Germany; Department of Chemical and Biological Engineering, Friedrich-Alexander-Universität Erlangen-Nürnberg, 91058 Erlangen, Germany*

Andreas Hutzler − *Forschungszentrum Jülich GmbH, Helmholtz Institute Erlangen-Nürnberg for Renewable Energy (IEK 11), 91058 Erlangen, Germany;* orcid.org/0000-0001-5484-707X

Thomas Böhm − *Forschungszentrum Jülich GmbH, Helmholtz Institute Erlangen-Nürnberg for Renewable Energy (IEK 11), 91058 Erlangen, Germany;* orcid.org/0000-0003-2036-2159

https://doi.org/10.1021/acsmaterialslett.3c00569
ACS Materials Lett. 2023, 5, 2039−2046

Simon Thiele − *Forschungszentrum Jülich GmbH, Helmholtz Institute Erlangen-Nürnberg for Renewable Energy (IEK 11), 91058 Erlangen, Germany; Department of Chemical and Biological Engineering, Friedrich-Alexander-Universität Erlangen-Nürnberg, 91058 Erlangen, Germany;* orcid.org/0000-0002-4248-2752

Complete contact information is available at: https://pubs.acs.org/10.1021/acsmaterialslett.3c00569

Author Contributions

All authors have approved the final version of the manuscript. CRediT: **Sebastian Auffarth** conceptualization, methodology, investigation, data curation, writing - original draft, visualization; **Maximilian Wagner** methodology, software, writing - review & editing; **Anja Krieger** investigation, visualization, writing - review & editing; **Birk Fritsch** investigation, visualization, writing - review & editing; **Linus Hager** conceptualization, writing - review & editing; **Andreas Hutzler** investigation, visualization, writing - review & editing; **Thomas Böhm** investigation, writing - review & editing; **Simon Thiele** funding acquisition, supervision, writing - review & editing; **Jochen Kerres** conceptualization, supervision, writing - review & editing

Notes

The authors declare no competing financial interest.

■ ACKNOWLEDGMENTS

The authors acknowledge financial support from the Bavarian Ministry of Economic Affairs, Regional Development and Energy.

■ ABBREVIATIONS

IEC, ion-exchange capacity; PPFS, polypentafluorostyrene; PWN-X, X% phosphonated polypentafluorostyrene; POS, polyoctylstyrene; STEM, scanning transmission electron microscope; EDXS, energy-dispersive X-ray spectroscopy; RAFT, reversible addition−fragmentation chain-transfer; NMR, nuclear magnetic resonance; GPC, gel permeation chromatograph; AIBN, azobisisobutyronitrile; DP, degree of polymerization; DDMAT, 2-(dodecylthiocarbonothioylthio)-2-methylpropanoic acid; DMSO, dimethylsulfoxide; THF, tetrahydrofuran; TSP, tris(trimethylsilyl)phosphite; HAADF, high-angle annular dark-field imaging; DMF, dimethylformamide; DMAc, dimethylacetamide; DSC, differential scanning calorimetry; SAED, selected area electron diffraction

■ REFERENCES

(1) Kerres, J. A. Design Concepts for Aromatic Ionomers and Ionomer Membranes to be Applied to Fuel Cells and Electrolysis. *Polymer Reviews* **2015**, *55*, 273−306.

(2) Chromik, A.; dos Santos, A. R.; Turek, T.; Kunz, U.; Häring, T.; Kerres, J. Stability of acid-excess acid−base blend membranes in all-vanadium redox-flow batteries. *J. Membr. Sci.* **2015**, *476*, 148−155.

(3) Park, J. E.; Kim, J.; Han, J.; Kim, K.; Park, S.; Kim, S.; Park, H. S.; Cho, Y.-H.; Lee, J.-C.; Sung, Y.-E. High-performance proton-exchange membrane water electrolysis using a sulfonated poly(arylene ether sulfone) membrane and ionomer. *J. Membr. Sci.* **2021**, *620*, 118871.

(4) Bernt, M.; Gasteiger, H. A. Influence of Ionomer Content in IrO_2/TiO_2 Electrodes on PEM Water Electrolyzer Performance. *J. Electrochem. Soc.* **2016**, *163*, F3179−F3189.

(5) Kerres, J. A. Development of ionomer membranes for fuel cells. *J. Membr. Sci.* **2001**, *185*, 3−27.

(6) Inaba, M.; Kinumoto, T.; Kiriake, M.; Umebayashi, R.; Tasaka, A.; Ogumi, Z. Gas crossover and membrane degradation in polymer electrolyte fuel cells. *Electrochim. Acta* **2006**, *51*, 5746−5753.

(7) Auffarth, S.; Dafinger, W.; Mehler, J.; Ardizzon, V.; Preuster, P.; Wasserscheid, P.; Thiele, S.; Kerres, J. Cross-linked proton-exchange membranes with strongly reduced fuel crossover and increased chemical stability for direct-isopropanol fuel cells. *J. Mater. Chem. A* **2022**, *10*, 17208−17216.

(8) Kreuer, K.-D.; Münchinger, A. Fast and Selective Ionic Transport: From Ion-Conducting Channels to Ion Exchange Membranes for Flow Batteries. *Annu. Rev. Mater. Res.* **2021**, *51*, 21−46.

(9) Banerjee, S.; Curtin, D. E. Nafion® perfluorinated membranes in fuel cells. *Journal of Fluorine Chemistry* **2004**, *125*, 1211−1216.

(10) Mališ, J.; Mazúr, P.; Paidar, M.; Bystron, T.; Bouzek, K. Nafion 117 stability under conditions of PEM water electrolysis at elevated temperature and pressure. *Int. J. Hydrogen Energy* **2016**, *41*, 2177−2188.

(11) Brodt, M.; Müller, K.; Kerres, J.; Katsounaros, I.; Mayrhofer, K.; Preuster, P.; Wasserscheid, P.; Thiele, S. The 2-Propanol Fuel Cell: A Review from the Perspective of a Hydrogen Energy Economy. *Energy Tech* **2021**, *9*, 2100164.

(12) Mauritz, K. A.; Moore, R. B. State of understanding of nafion. *Chemical Reviews* **2004**, *104*, 4535−4585.

(13) Roche, E. J.; Pineri, M.; Duplessix, R.; Levelut, A. M. Small-angle scattering studies of nafion membranes. *J. Polym. Sci. Polym. Phys. Ed.* **1981**, *19*, 1−11.

(14) Elabd, Y. A.; Napadensky, E.; Walker, C. W.; Winey, K. I. Transport Properties of Sulfonated Poly(styrene-b-isobutylene-b-styrene) Triblock Copolymers at High Ion-Exchange Capacities. *Macromolecules* **2006**, *39*, 399−407.

(15) Einsla, M. L.; Kim, Y. S.; Hawley, M.; Lee, H.-S.; McGrath, J. E.; Liu, B.; Guiver, M. D.; Pivovar, B. S. Toward Improved Conductivity of Sulfonated Aromatic Proton Exchange Membranes at Low Relative Humidity. *Chem. Mater.* **2008**, *20*, 5636−5642.

(16) Bosson, K.; Marcasuzaa, P.; Bousquet, A.; Tovar, G. E.; Atanasov, V.; Billon, L. PentaFluoroStyrene-based block copolymers controlled self-assembly pattern: A platform paving the way to functional block copolymers. *Eur. Polym. J.* **2022**, *179*, 111560.

(17) Bosson, K.; Marcasuzaa, P.; Bousquet, A.; Tovar, G. E.; Atanasov, V.; Billon, L. para fluoro-thiol clicked diblock-copolymer self-assembly: Towards a new paradigm for highly proton-conductive membranes. *J. Membr. Sci.* **2022**, *659*, 120796.

(18) Feng, S.; Voth, G. A. Proton solvation and transport in hydrated nafion. *The journal of physical chemistry. B* **2011**, *115*, 5903−5912.

(19) Lim, K. H.; Lee, A. S.; Atanasov, V.; Kerres, J.; Park, E. J.; Adhikari, S.; Maurya, S.; Manriquez, L. D.; Jung, J.; Fujimoto, C.; Matanovic, I.; Jankovic, J.; Hu, Z.; Jia, H.; Kim, Y. S. Protonated phosphonic acid electrodes for high power heavy-duty vehicle fuel cells. *Nat Energy* **2022**, *7*, 248−259.

(20) Arslan, F.; Chuluunbandi, K.; Freiberg, A. T. S.; Kormanyos, A.; Sit, F.; Cherevko, S.; Kerres, J.; Thiele, S.; Böhm, T. Performance of Quaternized Polybenzimidazole-Cross-Linked Poly(vinylbenzyl chloride) Membranes in HT-PEMFCs. *ACS Applied Materials & Interfaces* **2021**, *13*, 56584−56596.

(21) Pingitore, A. T.; Huang, F.; Qian, G.; Benicewicz, B. C. Durable High Polymer Content m/p -Polybenzimidazole Membranes for Extended Lifetime Electrochemical Devices. *ACS Appl. Energy Mater.* **2019**, *2*, 1720−1726.

(22) Kaserer, S.; Caldwell, K. M.; Ramaker, D. E.; Roth, C. Analyzing the Influence of H_3PO_4 as Catalyst Poison in High Temperature PEM Fuel Cells Using in-operando X-ray Absorption Spectroscopy. *J. Phys. Chem. C* **2013**, *117*, 6210−6217.

(23) Tang, H.; Gao, J.; Wang, Y.; Li, N.; Geng, K. Phosphoric-Acid Retention in High-Temperature Proton-Exchange Membranes. *Chemistry (Weinheim an der Bergstrasse, Germany)* **2022**, *28*, e202202064.

(24) Lim, K. H.; Matanovic, I.; Maurya, S.; Kim, Y.; Castro, E. S. de; Jang, J.-H.; Park, H.; Kim, Y. S. High Temperature Polymer Electrolyte Membrane Fuel Cells with High Phosphoric Acid Retention. *ACS Energy Lett.* **2023**, *8*, 529−536.

(25) Atanasov, V.; Kerres, J. Highly Phosphonated Polypentafluorostyrene. *Macromolecules* **2011**, *44*, 6416−6423.

(26) Nederstedt, H.; Jannasch, P. Poly(p-terphenyl alkylene)s grafted with highly acidic sulfonated polypentafluorostyrene side chains for proton exchange membranes. *J. Membr. Sci.* **2022**, *647*, 120270.
(27) Shao, Z.; Sannigrahi, A.; Jannasch, P. Poly-(tetrafluorostyrenephosphonic acid)-polysulfone block copolymers and membranes. *J. Polym. Sci. A Polym. Chem.* **2013**, *51*, 4657−4666.
(28) Yu, L.; Yue, B.; Yan, L.; Zhao, H.; Zhang, J. Proton conducting composite membranes based on sulfonated polysulfone and poly-sulfone-g-(phosphonated polystyrene) via controlled atom-transfer radical polymerization for fuel cell applications. *Solid State Ionics* **2019**, *338*, 103−112.
(29) Atanasov, V.; Gudat, D.; Ruffmann, B.; Kerres, J. Highly phosphonated polypentafluorostyrene: Characterization and blends with polybenzimidazole. *Eur. Polym. J.* **2013**, *49*, 3977−3985.
(30) Matsushima, S.; Takano, A.; Takahashi, Y.; Matsushita, Y. Precise synthesis of a series of poly(4-n-alkylstyrene)s and their glass transition temperatures. *J. Polym. Sci. Part B: Polym. Phys.* **2017**, *55*, 757−763.
(31) Funk, L.; Brehmer, M.; Zentel, R.; Kang, H.; Char, K. Novel Amphiphilic Styrene-Based Block Copolymers for Induced Surface Reconstruction. *Macromol. Chem. Phys.* **2008**, *209*, 52−63.
(32) Jankova, K.; Hvilsted, S. Preparation of Poly(2,3,4,5,6-pentafluorostyrene) and Block Copolymers with Styrene by ATRP. *Macromolecules* **2003**, *36*, 1753−1758.
(33) Atanasov, V.; Oleynikov, A.; Xia, J.; Lyonnard, S.; Kerres, J. Phosphonic acid functionalized poly(pentafluorostyrene) as polyelectrolyte membrane for fuel cell application. *Journal of Power Sources* **2017**, *343*, 364−372.
(34) Sun, X.; Guan, J.; Wang, X.; Li, X.; Zheng, J.; Li, S.; Zhang, S. Phosphonated Ionomers of Intrinsic Microporosity with Partially Ordered Structure for High-Temperature Proton Exchange Membrane Fuel Cells. *ACS Central Science* **2023**, *9*, 733−741.
(35) Vilčiauskas, L.; Tuckerman, M. E.; Bester, G.; Paddison, S. J.; Kreuer, K.-D. The mechanism of proton conduction in phosphoric acid. *Nature Chem* **2012**, *4*, 461−466.
(36) Atanasov, V.; Bürger, M.; Lyonnard, S.; Porcar, L.; Kerres, J. Sulfonated poly(pentafluorostyrene): Synthesis & characterization. *Solid State Ionics* **2013**, *252*, 75−83.
(37) Atanasov, V.; Lee, A. S.; Park, E. J.; Maurya, S.; Baca, E. D.; Fujimoto, C.; Hibbs, M.; Matanovic, I.; Kerres, J.; Kim, Y. S. Synergistically integrated phosphonated poly(pentafluorostyrene) for fuel cells. *Nat. Mater.* **2021**, *20*, 370−377.
(38) Elabd, Y. A.; Hickner, M. A. Block Copolymers for Fuel Cells. *Macromolecules* **2011**, *44*, 1−11.
(39) Bae, B.; Miyatake, K.; Watanabe, M. Synthesis and properties of sulfonated block copolymers having fluorenyl groups for fuel-cell applications. *ACS Applied Materials & Interfaces* **2009**, *1*, 1279−1286.
(40) Shi, Z.; Holdcroft, S. Synthesis and Proton Conductivity of Partially Sulfonated Poly([vinylidene difluoride-co-hexafluoropropylene]-b-styrene) Block Copolymers. *Macromolecules* **2005**, *38*, 4193−4201.
(41) Tsang, E. M. W.; Zhang, Z.; Shi, Z.; Soboleva, T.; Holdcroft, S. Considerations of macromolecular structure in the design of proton conducting polymer membranes: graft versus diblock polyelectrolytes. *J. Am. Chem. Soc.* **2007**, *129*, 15106−15107.
(42) Fritsch, B.; Wu, M.; Hutzler, A.; Zhou, D.; Spruit, R.; Vogl, L.; Will, J.; Hugo Pérez Garza, H.; März, M.; Jank, M. P. M.; Spiecker, E. Sub-Kelvin thermometry for evaluating the local temperature stability within in situ TEM gas cells. *Ultramicroscopy* **2022**, *235*, 113494.

https://doi.org/10.1021/acsmaterialslett.3c00569
ACS Materials Lett. 2023, 5, 2039−2046